Smart Mater. Struct. **2** (1993) 55–65. Printed in the UK

Aeroservoelastic DAP missile fin development*

Ron Barrett
NASA Space Grant Fellow, Aerospace Engineering Department, University of Kansas, Lawrence, Kansas, 66045-2221 USA

Received 8 January 1993, accepted for publication 12 April 1993

Abstract. The development of an active aeroservoelastic missile fin using directionally attached piezoelectric (DAP) actuator elements is detailed. Several different types of actuator elements are examined, including piezoelectric polymers, piezoelectric fiber composites and conventionally attached piezoelectric (CAP) and DAP elements. These actuator elements are bonded to the substrate of a torque plate. The root of the torque plate is attached to a fuselage hard point or folding pivot. The tip of the plate is bonded to an aerodynamic shell which undergoes a pitch change as the plate twists. The design procedures used on the plate are discussed. These include an optimization of the actuator element orientation, substrate material type and thickness, as well as a determination of the optimum elastic axis location. A comparison of the various actuator element shows that DAP elements provide the highest deflections with the highest torsional stiffness. A torque plate was constructed from 0.2032 mm thick DAP elements bonded to a 0.127 mm thick AISI 1010 steel substrate. The torque plate produced static twist deflections in excess of $\pm$ 3°. An aerodynamic shell with a modified NACA 0012 profile was added to the torque plate. This fin was tested in a wind tunnel at speeds up to 50 ms^{-1}. The static deflection of the fin was predicted to within 6% of the experimental data.

1. Introduction

Since aircraft flight control was first achieved by early glider enthusiasts, experimenters have sought ways of more effectively controlling aircraft with faster, lighter, smaller systems. Many of these developments have been in actuator design and integration of these improved actuators into more effective aerodynamic control surfaces. Missiles, like other aircraft, have seen better actuators develop over time. Currently, most of these actuator systems are pneumatic, hydraulic or electromechanical and occupy from 2 to 6% of fuselage volume. Because these actuators are mounted within the fuselage, they cannot be placed adjacent to critical components like rocket motors or seeker assemblies and they require bearings and linkages. Small missiles must use an extension tube aft of the rocket motor to accommodate these internal actuators [1,2]. They are also not amenable to some fin folding arrangements like those used on several types of unguided munitions [3]. Accordingly, there is a need for a type of inexpensive fin that occupies no fuselage volume and yet is capable of generating the forces and moments required for controlled flight.

A fin actuator that occupies no fuselage internal volume must be entirely contained within the aerodynamic shell of the fin. This presents problems for hydraulic and pneumatic systems, as current technology does not yet allow such miniaturization in a cost-effective manner. There is, however, a class of materials that may be capable of actuating such fins in the desired manner. Active materials have been shown to change the shape of beams and plates. If an active torque plate were integrated into a missile fin such that it could generate pitch deflections of the aerodynamic shell, then a simple type of solid state flight control actuator would result.

Several groups have investigated simple, solid state flight control surfaces using active materials. Crawley *et al* [4] were the first published authors to examine an active aeroservoelastic lifting surface using solid state actuator elements. They used conventionally attached lead zirconate titanate (PZT) piezoceramic sheets on a bending–twist coupled plate and subjected the plate to aerodynamic loading. They showed that extremely small amounts of active twist could be effectively magnified by the dynamic pressure of the air flow. Ehlers and Weisshaar [5] also investigated the effects of active aeroservoelasticity. They showed how adaptive materials can be used to control the aeroelastic properties of a uniform wing. Song *et al* [6] investigated the behaviour of an adaptive aeroelastic wing modeled as a thin-walled beam. Spangler and Hall [7] investigated the performance of a rotor blade using a piezoelectrically actuated conventional flap. Spangler and Hall concluded that

* Presented at the Third International Conference on Adaptive Structures, San Diego, California, 9–11 November 1992.

0964-1726/93/020055 + 11 $7.50

piezoelectrically actuated flaps are capable of generating significant aerodynamic forces, and their experiment confirmed that conclusion. Lazarus *et al* [8] examined the performance of low-aspect-ratio wings using active camber and twist control. A study performed by Ehlers and Weisshaar [9] examined the effect of material properties on aeroelastic control. They analyzed several different types of actuator materials, including PVDF film, piezoelectric fiber composites, CAP and DAP elements. They showed that when torsional actuation is important to an adaptive structure, highly orthotropic actuator elements provide the greatest degree of actuation. Of the materials examined, DAP elements generated deflections and moments that were double those of other materials. Ehlers and Weisshaar's work built upon some of the basic proof-of-concept studies into DAP materials conducted by Barrett [10–12] and continued by Chopra [13]. These basic studies were expanded to more advanced configurations of actuator devices and lamination schemes. Configurations of active subsonic and supersonic missile fins were tested by Barrett [14–16]. This paper will build upon the subsonic missile wing configuration and further establish the actuator and substrate material selection, analysis and design procedures.

2. Actuator material analysis

The properties of the four actuator materials will first be examined. Foremost among these properties are the actuator strain rates and stiffnesses. The piezoelectric polymer polyvinylidene flouride (PVDF) and CAP elements require no approximations to obtain their stiffnesses. DAP elements and piezoelectric fiber composites, however, require some estimation.

PVDF has relatively low isotropic stiffness characteristics. However, it does exhibit differing actuation strains in the longitudinal and lateral directions and can accordingly be used to actuate beams and plates in torsion. PVDF is amenable to lamination and has successfully been bonded to many structures.

PZT elements have significantly higher isotropic stiffness and often exhibit nearly equal in-plane strains. Piezoelectric fiber composites, like the conventional PZT sheets, are simple to analyze. Using methods outlined by Jones [17] and Ekvall [18] the longitudinal and lateral stiffnesses and the actuation strains are obtained by some fundamental approximations that account for the triaxial state of stress in the matrix due to fiber restraint:

$$\Lambda_L \cong \frac{\Lambda E_f V_f}{V_f E_f + V_m E_m} \tag{1}$$

$$\Lambda_T \cong \Lambda V_f \tag{2}$$

$$E_L \cong E_f V_f + \frac{E_m V_m}{(1 - 2\nu_m^2)} \tag{3}$$

$$E_T \cong \frac{E_f E_m}{V_f E_m + V_m E_f (1 - 2\nu_m^2 (1 - \nu_m^2)} \tag{4}$$

$$\nu_{LT} \cong \nu_f V_f + \nu_m V_m \tag{5}$$

$$G_{LT} \cong \frac{G_f G_m}{V_m G_f + V_f G_m}. \tag{6}$$

To successfully predict the effective stiffnesses of directionally attached actuator elements, three effects must be considered: (i) partial attachment, (ii) transverse shear lag, and (iii) differential stiffness bonding. The goal of directional attachment is to make an isotropic or nearly isotropic actuator element behave as if it were highly orthotropic. To do this, the elements are bonded so that they are allowed to expand and contract freely in the lateral direction, while being firmly joined to the substrate in the longitudinal direction. The first embodiment of directional attachment is partial attachment. A central portion of the element is bonded to the substrate, while the sides are left free and unattached. Figure 1 shows a schematic diagram of this attachment arrangement. To estimate the modifications to the effective stiffnesses, the following are shown by Barrett [15] to be reasonable approximations:

$$E_{Leffo} = E_{Lo}\left(\frac{L_{effo}}{L_o} - \frac{(W_o - W_{effo})^2}{2L_o W_o}\right) \tag{7}$$

$$E_{Teffo} = E_{To}\int_0^{L_o} \frac{W_{effo}(x)}{W_o L_o}\,dx. \tag{8}$$

The original effective stiffnesses, E_{Leffo} and E_{Teffo}, are functions of the attachment geometry. Equations (7) and (8) account for the areas of the active elements that participate in strain actuation in the longitudinal and lateral directions respectively. These equations are improvements on earlier models developed by Barrett [10, 11]. They allow for prediction of effective stiffnesses of elements with attachment areas that have shapes other than rectangular. There are numerous different attachment patterns that have been explored. The original proof-of-concept beams used rectangular attachment areas that were from 1/4 to 1/3 of the width of the actuator element as shown in figure 1. It was found that the smaller the lateral attachment area, the higher the orthotropy. More advanced attachment areas use inverse ellipse attachment areas to eliminate stress risers

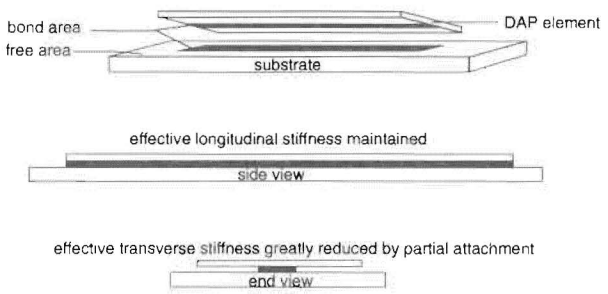

Figure 1. Partial attachment schematic [10].

that initiate de-bonds and yet maintain the high degree orthotropy.

The second embodiment of directional attachment is the use of transverse shear lag. From a finite thickness bond, shear lag will degrade the effective stiffnesses both in the longitudinal and lateral directions. Equation (9) below approximates the effects of longitudinal shear lag that the element experiences from a finite thickness bond. A similar approximation for the transverse shear lag can be obtained from equation (9) by examining the transverse stiffness instead of the longitudinal stiffness and the width instead of the length. This shear lag will generally enhance the orthotropy of an actuator element. This simple approximation has been shown to hold for DAP elements with bond pattern aspect ratios greater than 2 [10].

$$\frac{E_{\mathrm{Leff}}}{E_{\mathrm{Leffo}}} = \sinh^{-1}\left\{\frac{\sinh}{2}\left[\left(\frac{L_{\mathrm{effo}}}{2}\right)\sqrt{\frac{G_{\mathrm{b}}}{t_{\mathrm{a}}t_{\mathrm{b}}E_{\mathrm{a}}}}\right]\right\} \times \left[\left(\frac{L_{\mathrm{effo}}}{2}\right)\sqrt{\frac{G_{\mathrm{b}}}{t_{\mathrm{a}}t_{\mathrm{b}}E_{\mathrm{a}}}}\right]^{-1}. \tag{9}$$

The terms of equations (7), (8) and (9) are defined by the geometry laid out in figure 2.

The final embodiment of directional attachment comes from differential stiffness bonding. This is primarily a manufacturing modification that adds stiff bond material on the longitudinal ends of the actuator elements. This enhances the orthotropy, helps to prevent de-bonds, provides protection for the leads and helps to retard arcing around the ends of the element. The added orthotropy, although present, is very small, difficult to measure and difficult to predict. Accordingly, in most cases, it is acceptable to make no further modifications to the effective stiffnesses as long as an end-bonding agent like epoxy is used [15]. If end-bonded plates are made from a stiff material like aluminum, brass or steel, then modifications to the effective moduli should be made. $E_{\mathrm{Leff}}/E_{\mathrm{Lo}}$ will be increased from 94–98% to $\sim$ 100%.

There exists another method of manufacturing that improves the orthotropy, strain rate and stiffness of directionally attached actuator elements. This manufacturing technique is called directional enhancement and is outlined in [15]. Directional enhancement will not be covered in this paper, but the reader should be aware that the performance of DAP elements can be enhanced by 6 to 20% through this method.

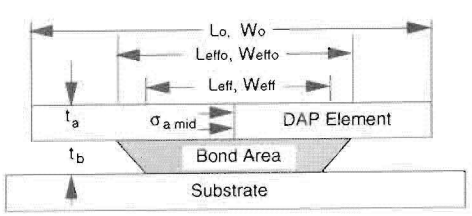

Figure 2. DAP attatchment schematic [10].

2.1. Laminated plate models

Classical laminated plate theory will be used to analyze and compare the various types of actuator materials and substrates. The model assumes constant in-plane strain through the thickness and bending strains are linearly varying through the thickness of the plate. The model uses the formulation employed by Jones [17] to predict thermally induced strains in lamina. The strains of the laminate can be cast in terms of the mid-plane strains and curvatures. Following Jones [17], the relationship between the externally applied forces and moments, the laminate stiffness and the actuation strain-induced forces and moments follow:

$$\begin{Bmatrix} N \\ M \end{Bmatrix} = \begin{bmatrix} \mathbf{A} & \mathbf{B} \\ \mathbf{B} & \mathbf{D} \end{bmatrix}_{\mathrm{l}} \begin{Bmatrix} \epsilon^0 \\ \kappa \end{Bmatrix} - \begin{Bmatrix} N \\ M \end{Bmatrix}_{\mathrm{a}}. \tag{10}$$

The stiffness matrix is composed of the reduced stiffnesses of each ply in the laminate axes. The applied forces and moments per unit length are integrated through the thickness of the plate and are defined as follows:

$$N = \int \sigma \mathrm{d}z \qquad M = \int \sigma Z \mathrm{d}z. \tag{11}$$

Modeling the active elements is fairly simple. For a general orthotropic active element in the laminate axes that is capable of generating only in-plane strains as a free element (as is the case with all of the elements considered), the actuation strain vector can be obtained as follows:

$$\begin{Bmatrix} N \\ M \end{Bmatrix}_{\mathrm{a}} = \begin{bmatrix} \mathbf{A} & \mathbf{B} \\ \mathbf{B} & \mathbf{D} \end{bmatrix}_{\mathrm{a}} \begin{Bmatrix} \Lambda_\epsilon \\ \Lambda_\kappa \end{Bmatrix} = [N_{11}N_{22}N_{12}M_{11}M_{22}M_{12}]_{\mathrm{a}}^{\mathrm{T}}. \tag{12}$$

Since CAP elements are isotropic and generate approximately the same actuation strains in both directions, the actuator matrix will have zeros at the shear and twist induction terms. This indicates that if CAP elements are used, a coupled substrate must be present if any twist or shear is to be generated. Although PVDF also has an isotropic stiffness matrix, the active strains Λ_1 and Λ_2 are not equal. Because they are not equal, they will generate in-plane shear strains when they are oriented at angles off the laminate axes. The same argument holds for the analysis of piezoelectric fiber composites, but both the actuator strains and the stiffnesses are unequal in the longitudinal and lateral directions. Like PVDF, the piezoelectric fiber composite will be able to generate shear and twist in either coupled or uncoupled lamina. DAP elements can be modeled as having equal longitudinal and lateral strain rates, but have differing longitudinal and lateral stiffnesses. Accordingly, PVDF, piezoelectric fiber composites and DAP elements can be artificially given a d_{36} property by rotating the actuator ply. As a result, they have an added dimension of structural control over CAP elements.

2.2. Analysis of an active laminate with two DAP plies

To get an idea of how the DAP elements perform on an uncoupled substrate, solutions for the laminate strains will be derived. Assuming that the laminate is composed of three components with the sequence [+ΘDAP(+Λ)/uncoupled substrate/+ΘDAP(−Λ)], and taking the opposite actuation strains on the upper active element and lower active element, a bending–twist coupled motion will result. The strains and curvatures for this laminate are as follows

$$\epsilon_{11} = \epsilon_{22} = \epsilon_{12} = 0 \tag{13}$$

$$\begin{aligned}\kappa_{11} = \{&[(D_{12}D_{26} - D_{22}D_{16})_1(B_{16} + B_{26})_a \\ &+ (D_{22}D_{66} - D_{26}^2)_1(B_{11} + B_{12})_a \\ &+ (D_{16}D_{26} - D_{12}D_{66})_1 \\ &\times (B_{22} + B_{12})_a]/[(D_{11}D_{22} - D_{12}^2)_1 D_{661} \\ &+ (D_{12}D_{26} - D_{22}D_{16})_1 D_{161} \\ &+ (D_{12}D_{16} - D_{11}D_{26})_1 D_{261}]\}\Lambda\end{aligned} \tag{14}$$

$$\begin{aligned}\kappa_{22} = \{&[(D_{12}D_{16} - D_{11}D_{26})_1(B_{16} + B_{26})_a \\ &+ (D_{11}D_{66} - D_{26}^2)_1(B_{22} + B_{12})_a \\ &+ (D_{16}D_{26} - D_{12}D_{66})_1 \\ &\times (B_{11} + B_{12})_a]/[(D_{11}D_{22} - D_{12}^2)_1 D_{661} \\ &+ (D_{12}D_{26} - D_{22}D_{16})_1 D_{161} \\ &+ (D_{12}D_{16} - D_{11}D_{26})_1 D_{261}]\}\Lambda\end{aligned} \tag{15}$$

$$\begin{aligned}\kappa_{12} = \{&[(D_{11}D_{22} - D_{12}^2)_1(B_{16} + B_{26})_a \\ &+ (D_{12}D_{26} - D_{22}D_{16})_1(B_{11} + B_{12})_a \\ &+ (D_{12}D_{16} - D_{11}D_{26})_1 \\ &\times (B_{22} + B_{12})_a]/[2((D_{11}D_{22} - D_{12}^2)_1 D_{661} \\ &+ (D_{12}D_{26} - D_{22}D_{16})_1 D_{161} \\ &+ (D_{12}D_{16} - D_{11}D_{26})_1 D_{261})]\}\Lambda\end{aligned} \tag{16}$$

If the top and bottom active layers are arranged antisymmetrically and both plies are activated in phase with the sequence [+ΘDAP(+Λ)/uncoupled substrate/−ΘDAP(+Λ)], then an extension–twist coupled motion will result. The strains and curvatures are as follows:

$$\begin{aligned}\epsilon_{11} = \{&[(A_{12}B_{26} - A_{22}B_{16})_1(B_{16} + B_{26})_a \\ &+ (A_{22}D_{66} - B_{26}^2)_1(A_{11} + A_{12})_a + (B_{16}B_{26} - A_{12}D_{66})_1 \\ &\times (A_{22} + A_{12})_a]/[(A_{11}A_{22} - A_{12}^2)_1 D_{661} \\ &+ (A_{12}B_{26} - A_{22}B_{16})_1 B_{161} \\ &+ (A_{12}B_{16} - A_{11}B_{26})_1 B_{261}]\}\Lambda\end{aligned} \tag{17}$$

$$\begin{aligned}\epsilon_{22} = \{&[(A_{12}B_{16} - A_{11}B_{26})_1(B_{16} + B_{26})_a \\ &+ (A_{11}D_{66} - B_{16}^2)_1(A_{22} + A_{12})_a + (B_{16}B_{26} - A_{12}D_{66})_1 \\ &\times (A_{11} + A_{12})_a]/[(A_{11}A_{22} - A_{12}^2)_1 D_{661} \\ &+ (A_{12}B_{26} - A_{22}B_{16})_1 B_{161} \\ &+ (A_{12}B_{16} - A_{11}B_{26})_1 B_{261}]\}\Lambda\end{aligned} \tag{18}$$

$$\epsilon_{12} = \kappa_{11} = \kappa_{22} = 0 \tag{19}$$

$$\begin{aligned}\kappa_{12} = \{&[(A_{11}A_{22} - A_{12}^2)_1(B_{16} + B_{26})_a \\ &+ (A_{12}B_{26} - A_{22}B_{16})_1(A_{11} + A_{12})_a \\ &+ (A_{12}B_{16} - A_{11}B_{26})_1(A_{22} + A_{12})_a] \\ &/2((A_{11}A_{22} - A_{12}^2)_1 D_{661} \\ &+ (A_{12}B_{26} - A_{22}B_{16})_1 B_{161} \\ &+ (A_{12}B_{16} - A_{11}B_{26})_1 B_{261})]\}\Lambda.\end{aligned} \tag{20}$$

If the denominators of the reduced stiffnesses are assumed to be approximately equal, $(1 - \nu_{LTa}\nu_{TLa} \cong 1 - \nu_s^2)$ and the DAP elements are attached at ±45° from the longitudinal axis with no bond thickness, then equation (20) can be solved directly for the twist of the laminate:

$$\begin{aligned}\kappa_{12} = &[(E_s t_s(1 + \nu_s))(E_{Ta} - E_{La})(t_s t_a + t_a^2)\Lambda] \\ &/[E_s t_s(1 + \nu_s) + (E_{La} + E_{Ta} + 2E_{La}\nu_{TL})t_a] \\ &\times \{[E_s t_s^3(1 - \nu_s)/6] + (E_{La} + E_{Ta} - 2E_{La}\nu_{TL}) \\ &\times [(t_s^2 t_a/2) + t_s t_a^2 + (2t_a^3/3)]\} \\ &- \tfrac{1}{2}[(t_s t_a + t_a^2)(E_{La} - E_{Ta})]^2\}.\end{aligned} \tag{21}$$

Errors from 1 to 5% in twist rate estimation will be induced by the assumption that the denominators of the reduced stiffnesses are approximately equal. Also, the assumption that the bond line is infinitely thin is fairly good when the bond line is less than an order of magnitude smaller than both the substrate and the actuator element.

2.3. Estimation of active laminate properties

From manufacturers' data, the properties of PVDF [19] and PZT [20] are obtained. Using the characteristics of PZT, and iterating about fiber volume fraction to optimize the twist generation capability, the characteristics of a hypothetical piezoelectric fiber composite with $V_f = 55\%$ can be obtained using equations (1)–(6). Using the characteristics of PZT and the geometry of figure 3, an estimation for the stiffnesses of a DAP laminate can be obtained. The bond area is tailored in the form of an inverse ellipse with a thickness of 0.0508 mm. A summary of the actuator stiffnesses, maximum strain rates and ultimate strains is given in table 1.

The strain rates Λ_{11}^* and Λ_{22}^* are the maximum recommended values so that depoling will be avoided. The stiffnesses and strains shown in table 1 are used to estimate the performances of the PVDF, piezo-fiber and DAP lamina. They have a sequence of [+45° active ply(+Λ)/steel/−45° active ply(+Λ)]. The CAP elements are bonded to a hypothetical extension–twist coupled graphite laminate of AS1/3506-1. The CAP laminate has the following sequence: [CAP(+Λ)/ + 45°AS1/−45°AS1/CAP(+Λ)]. To compare the actuator material's ability to induce twist in the laminate, it will be assumed that each laminate has a passive torsional stiffness, M_{12}/κ_{12}, of 1 N m rad^{-1}.

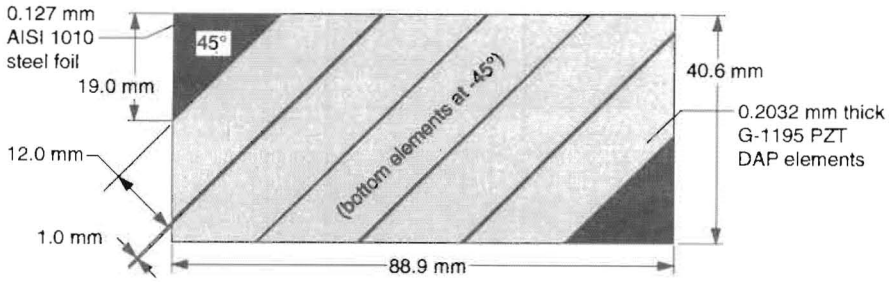

Figure 3. DAP laminate geometry.

Figure 4 shows the required thicknesses of the elements and the steel substrate to meet this stiffness. As will be shown later, a steel substrate provides higher deflections than most others because of its 205 GPa stiffness. The torsional stiffness has been chosen to be the normalizing quantity for plate comparison. This is because the plate torsional stiffness can be shown to affect the flutter and divergence speeds of the torque plate fin. (Plate mass is not a major concern as it will be shown to be less than 1/5 of the mass of the fin structure.)

The large thickness of the PVDF actuator plies shown in figure 4 can be attributed to an extremely low modulus of 2 GPa. Figures 5 and 6 show the masses of the lamina, the free twist rates and the restrained moments. Figure 5 shows that the DAP and CAP lamina weigh more than the others. This is primarily due to the high density of the PZT elements. Figure 6 shows that the active performance of the DAP laminate is far greater than the other lamina. The next closest competitor to the DAP laminate is the piezoelectric fiber composite. The DAP laminate produces deflections and restrained moments that are 32% higher than the piezoelectric fiber composite with a 30% increase in weight. This is due to the high density of the DAP elements. These results are similar to those produced by Ehlers and Weisshaar [9] for actuation of a uniform wing.

3. Active aeroservoelastic missile fin development

3.1. Fin design procedures

The design process used to create the active aeroservoelastic missile fin will now be detailed. In general, missile fin geometries and control deflection criteria are fixed by flight dynamicists, aerodynamicists and designers. The structures are then designed to meet those criteria. In an attempt to mimic this design process, a generic NACA 0012 airfoil section was selected with a $\pm 10°$ design pitch deflection.

From the previous section, the most suitable actuator material type will be chosen. There are four major justifications for using the DAP elements over the other torque-plate actuator materials. The driving normalizer for comparison was the torsional stiffness of the actuator plates. This torsional stiffness is the major parameter that affects the fluter and divergence speeds of the fin.

(i) For equal torsional stiffnesses, the DAP elements generate twist deflections that are more than 32% higher than any of the other actuator element types.

(ii) DAP elements also generate restrained moments that are more than 32% higher than any other actuator type.

(iii) Mass is of lesser importance because the weight of the torque plate is less than 1/5 of the total mass of the structure and less than 1/10 of the modal mass in first torsion.

Accordingly, even though the DAP elements are one of the most dense actuator types, the 30% increase in mass over other actuator types leads to a degradation of flutter speed by less than 3% and an increase in fin weight by only 6%.

(iv) The high volumetric actuator density of the DAP elements allows them to be arranged more favorably within the tight geometric confines of the fin shell.

To choose a suitably sized specimen for the proof-of-concept study, the maximum dimensions available from standard PZT sheets were chosen. This resulted in a torque plate with the dimensions of figure 3. The rest

Table 1. Plate material properties.

	L (mm)	W (mm)	E_L (GPa)	E_T (GPa)	G_{LT} (GPa)	ϵ_{ult} (μstrain)	Λ_{11}^* (μstrain)	Λ_{22}^* (μstrain)	ρ (g cm^{-3})	t (mm)
Steel substrate	n/a	n/a	205	205	77.0	2170	0	0	7.87	var.
Bond	n/a	n/a	23.4	23.4	8.8	n/a	0	0	n/a	0.0508
PVDF	n/a	n/a	2	2	0.75	27 500	231	30.5	1.25	var
PZT-CAP	n/a	n/a	63	63	23.7	1 200	220	220	7.65	var.
PZT-fiber comp.	n/a	n/a	37.5	14.0	3.8	1 200	207	121	4.82	var.
PZT-DAP original	53.9	12.0	63	63	23.7	1 200	220	220	7.65	var.
effo	49.8	2.04	58.19	10.72	21.88					
eff	49.2	1.46	57.55	7.70	21.63					

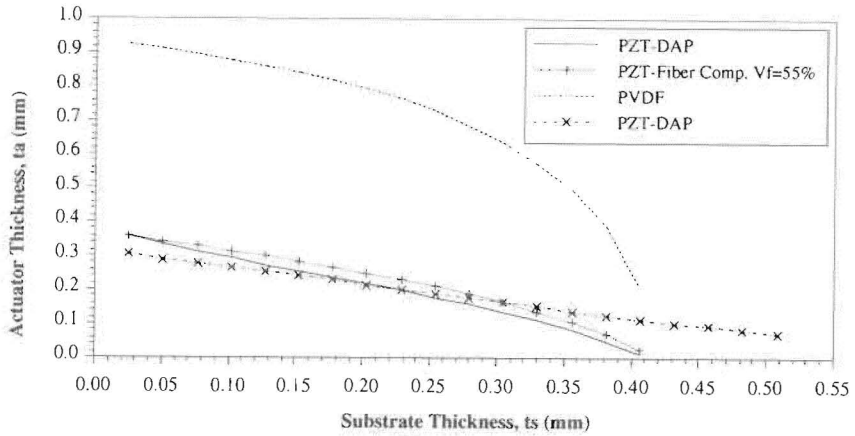

Figure 4. Required thicknesses for 1 N M rad torsional stiffness.

of the design procedure was composed of four major sections:

(i) Determination of activation ratio boundary so as to prevent actuator breakage.

(ii) Iteration of torque plate characteristics to arrive at the highest plate stiffness.

(iii) Determination of additional stiffness from adding a spar and root mount.

(iv) Determination of the optimum placement of the spar to achieve flight control.

3.2. Determination of the activation ratio, κ_{12}/Λ, boundary

From the given geometry and 10° pitch deflection criterion, the entire plate twist rate is 1.96 rad m^{-1}. With an actuator surface area density of 88%, the required actuator twist rate is 1.72 rad m^{-1}. From manufacturers' data, the ultimate strain rate is 1200 μstrain statically. For design purposes, a safety factor of 2 is chosen. Accordingly, to keep the elements from breaking, the minimum activation ratio that the torque plate must have is 2.87 rad (m mstrain)$^{-1}$.

3.3. Determination of the torque plate characteristics to arrive at the highest plate stiffness

A high plate stiffness is necessary for a high break frequency and retardation of flutter. Accordingly, the plate that has the highest torsional stiffness will be used. Since the weight of the plate will be shown to be less than 24% of the weight of the fin, the torque plate will not be a design driver. Accordingly, the activation ratio and torsional stiffness will drive the design. From figure 6 and table 1 it is clear that DAP elements have an activation ratio that is more than 32% higher than that of any of the other actuator elements. Also, DAP elements are very inexpensive, easily mass produced, and have been proven through more than three years of research. (Piezo-fiber composites are still in the basic stages of development and will cost significantly more than DAP elements once they are available.) Accordingly, DAP elements will be chosen for the fin design. To optimize the DAP actuators, an evaluation of the actuator substrate materials must be made. Because only 0.232 mm thick PZT sheets were readily available, iteration about actuator thickness was not possible, but should be performed in a more well funded study. To determine the suitability of using an extension–twist coupled AS1/3506-1 graphite/epoxy substrate, a study of the optimum ply orientation was conducted. At the optimum substrate thickness of 0.127 mm, figure 7 shows that the optimum ply orientation falls at 45° for both the substrate and the DAP plies. Figure 8 goes further to show where the DAP/graphite–epoxy laminate falls with respect to other materials. Figure 8 was constructed with DAP elements laminated at ±45° on the substrate (the optimum lamination angle).

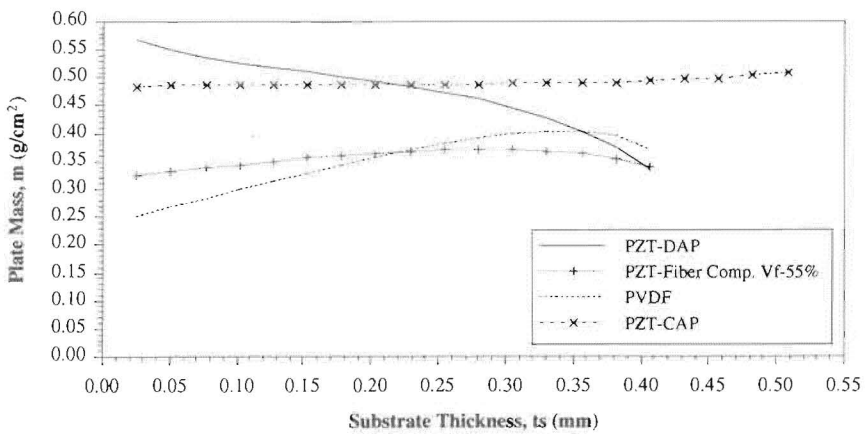

Figure 5. Comparison of plate masses.

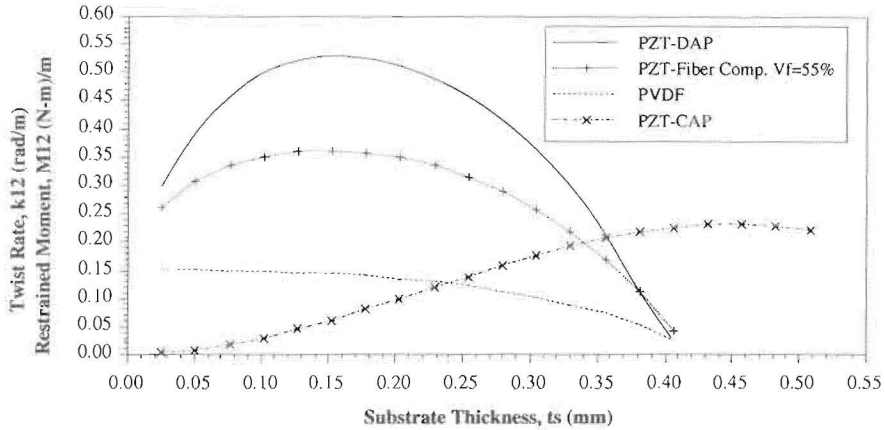

Figure 6. Comparison of plate-restrained moments and twist rates.

3.4. Determination of the wing spar and root attachment design

Given the design flight speed of 120 m s^{-1}, the wing spar was designed from two plies of Thornel^{TM} P-75 unidirectional graphite fibers laminated perpendicular to the torque plate. At the plate root, a steel strap constructed from 0.127 mm thick AISI 1010 steel foil was added. The steel strap, graphite spar and torque plate were epoxied to an aluminum base with Hexcel Safe-T-Poxy^{TM} in a room-temperature cure. The wing spar and airfoil configuration are shown in figure 9. The wing spar and root attachment increased the torsional stiffness of the torque plate from 0.506 to 0.788 N m rad^{-1}. This acted to degrade the static deflections and increase the break frequency of the fin.

3.5. Determination of the elastic axis location

The elastic axis will be placed at a position so that the maximum design deflection of 10° will be achieved in level flight with active control driving the fin towards the maximum deflection angle. Equation (22) gives an approximation for the aeroservoelastic angle of attack as a function of design parameters:

$$e = \frac{K_{tot}\alpha_e + K_a \Lambda}{qscC_{L\alpha}(\alpha_e + \alpha_o)}. \tag{22}$$

With $C_{L\alpha} \cong 0.056$ deg^{-1}, $K_{tot} = 0.788$ N m, rad^{-1}, $K_a = 0.0001733$ N m μstrain^{-1}, $\alpha_o = 0$, $\alpha_e = 10°$ and $V = 120$ m s^{-1} at sea-level with the geometry of figure 9, the elastic axis is set at 30% of the chord behind the leading edge (30%c). Accordingly, the design of the active aeroservoelastic fin is now fixed.

These design procedures are obviously intermingled with experimentally gathered data. This was necessary as some parameters were nearly impossible to predict, like the added stiffness due to the spar and root attachment. The lift-curve slope was also experimentally gathered for the static wing shell. Although not as elegant as analytical solution methods, it is significantly more accurate given the unique shape of the airfoil section.

3.6. Fin construction

The aeroservoelastic fin was built in three stages. First the torque plate was built, then the spar and end con-

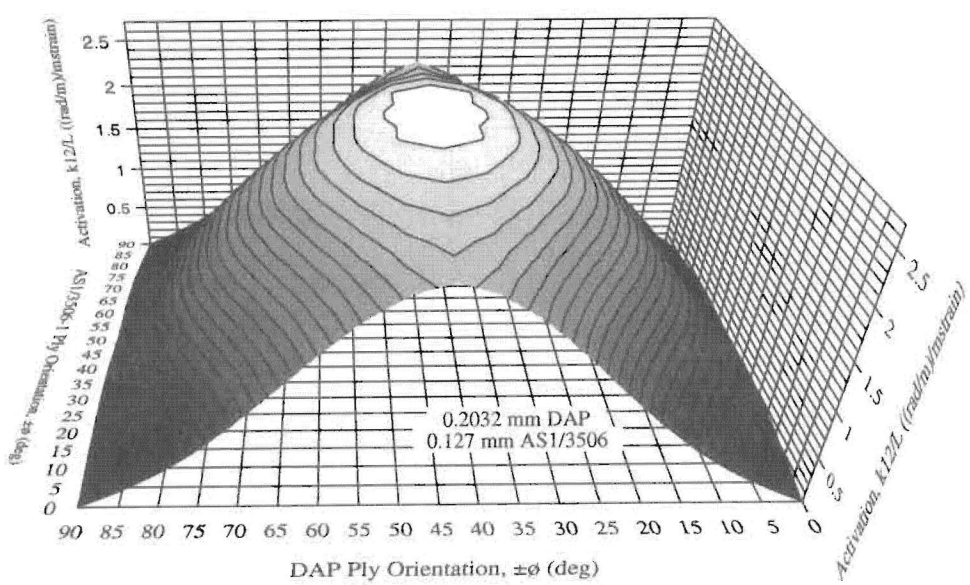

Figure 7. Activation ratio as a function of ply orientation.

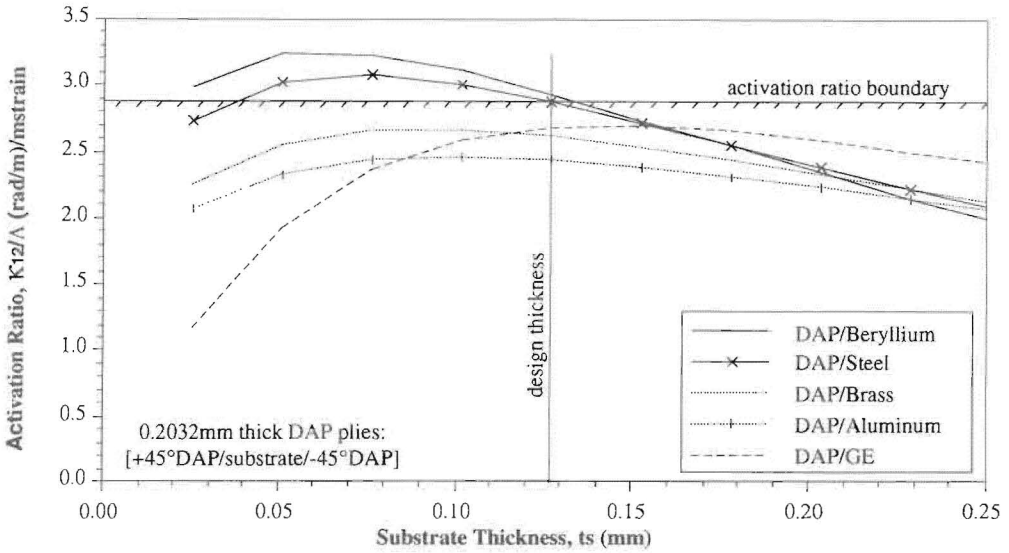

Figure 8. Activation ratio with various substrate materials.

nector were added, then the assembly was integrated in a hollow graphite/epoxy aerodynamic shell. The DAP torque plate was built of two major components, 0.2032 mm thick G-1195 PZT actuator elements and 0.127 mm thick AISI 1010 steel foil. The pre-poled PZT elements were cut to ±0.2 mm tolerance to the geometry of figure 3 on an abrasive cutting table using a wet cutting process. The elements were then cleaned with propanol to remove any oils or acids. The elements were laid up in an assembly jig and 0.0254 mm thick siliconized parting plies were added on the underside of the elements. The top sides of the elements also had parting plies as seen in figure 10. After the parting plies were added and the ends were sealed, 0.0254 mm thick brass leads were soldered on the open surfaces of the elements. After soldering, the elements were again cleaned with acetone and doped with Hexcel Safe-T-Poxy. The elements were joined to the substrate under approximately 20 psig of pressure and cured at room temperature. The other side was laid up in an identical manner.

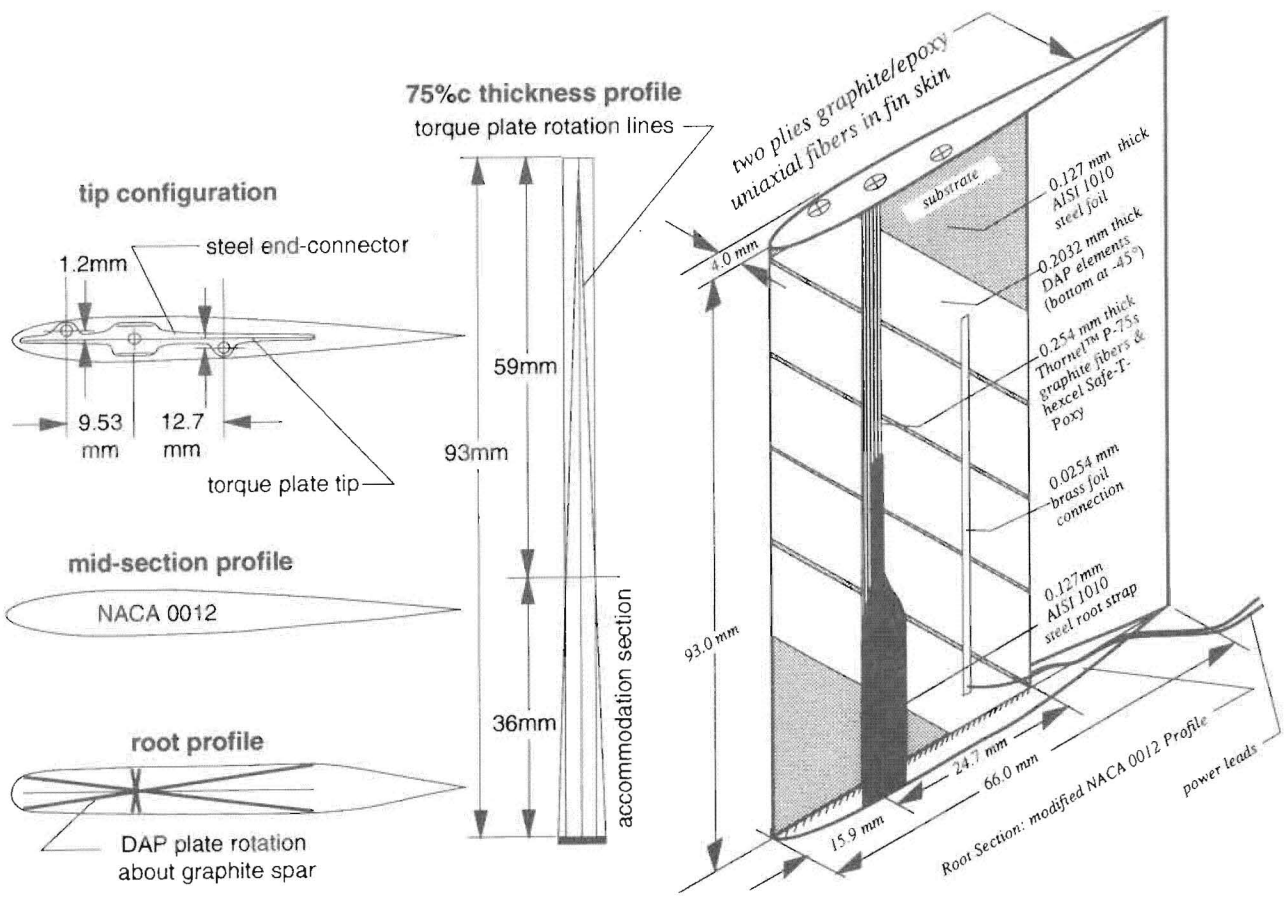

Figure 9. DAP torque plate and fin geometry.

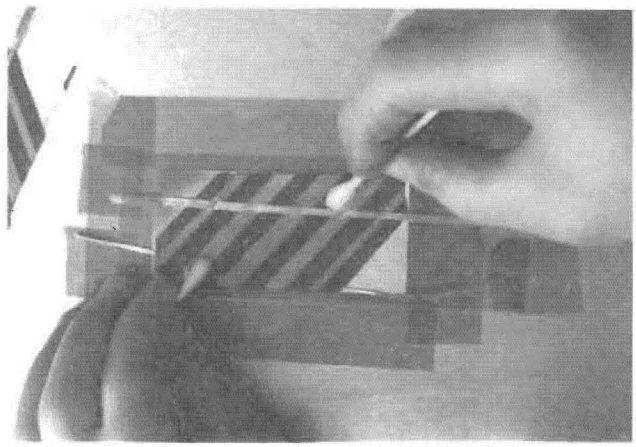

Figure 10. DAP elements on steel substrate prior to bonding.

After integration of the DAP elements to the substrate, the torque plate was tested for stiffness and deflection. Following the tests, the plate received a Thornel^{TM} P-75s graphite spar, a 0.127 mm thick steel root strap, and an end connector. The torque plate was then epoxied to a 2024-T3 aluminum test base. Following this, the torque plate was again tested for deflection and stiffness. An aerodynamic shell composed of two uniaxial P-75s graphite/epoxy plies was built to the configuration shown in Figure 9. This aerodynamic shell was bonded to a 2024-T3 aluminum end plate which was fastened to the steel end-connector of the torque plate.

3.7. Fin and torque plate testing

The torque plate was tested for static deflection before any modifications were made. The deflections of the plate were measured by reflecting a laser off a mirror that was fixed on the surface of the plate. The deflections were predicted using equation (21) with verification of a laminated plate code. Figure 11 shows the correlation of theory and experiment for the plate. After the testing of the clean plate was completed, the plate was again tested with the spar, root strap and end connector. The plate was tested for stiffness and it was determined that the plate had a torsional stiffness of 0.788 N m rad^{-1}. This new passive value was used to predict the performance of the wing in the wing tunnel.

The wing was tested in the 0.762 m × 0.533 m subsonic wind tunnel at the University of Kansas Aerospace Engineering Department. The fin was mounted on a flat plate which was anchored to the balance. Testing was conducted to determine active deflection as a function of airspeed up to 50 m s^{-1}. Figure 12 shows the fin undergoing deflections in the wind tunnel at 40 m s^{-1} airspeed. During testing, there was a significant amount of creep as the loading increased. This is due to the inherent characteristics of the PZT actuator elements. (Directionally attached electrostrictive elements would eliminate this problem.)

Using the DAP prediction methods and equation (22), the static deflection of the DAP fin was determined. Figure 13 shows the deflection as a function of airspeed. The correlation of theory and experiment are not as good as that for the torque plate. However, the results are still within 6% of each other. It should be noted that there were several possible sources of experimental error, including poor force resolution on the balance, turbulent flow in the test section and poor-grade Plexiglass in the tunnel walls. The test data shown in figure 13 display the results of statically pitching the airfoil to an angle of attack of 5°, then energizing and recording the results of the active pitch angle about the 5° baseline. It is clear that curves are shifted by the dynamic pressure, but the amount of control that the wing retains is approximately constant.

4. Conclusions

It can be concluded that of the four types of actuator materials examined, PVDF, CAP, piezo composites and DAP elements, DAP elements generate the highest deflections and constrained torsional moments on a plates with the same passive stiffness. DAP elements generate 32% more deflection and constrained torsional moment than the next closest actuator material, piezoelectric polymers. DAP elements and CAP elements bonded to a coupled substrate weight more than piezoelectric fiber composites by approximately 30%. The deflections of the DAP lamina can be predicted using simple approximation methods that account for directional attachment by modifying the effective stiffness of the DAP plies.

The orientation angle of an extension–twist coupled laminate that provides the highest torsional deflections is

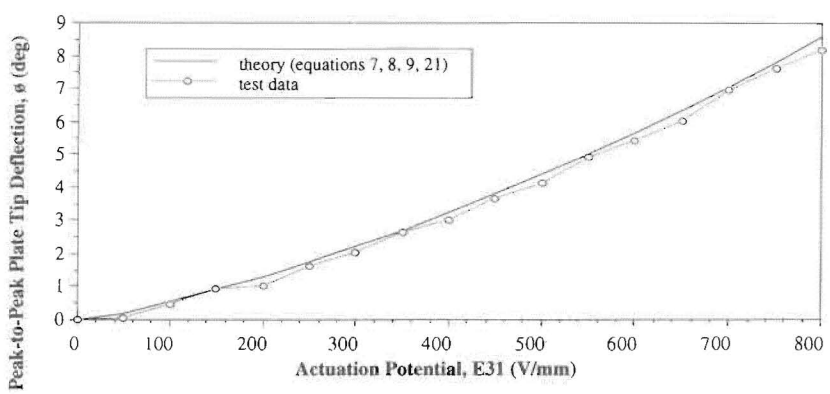

Figure 11. DAP torque plate twist prediction and experiment.

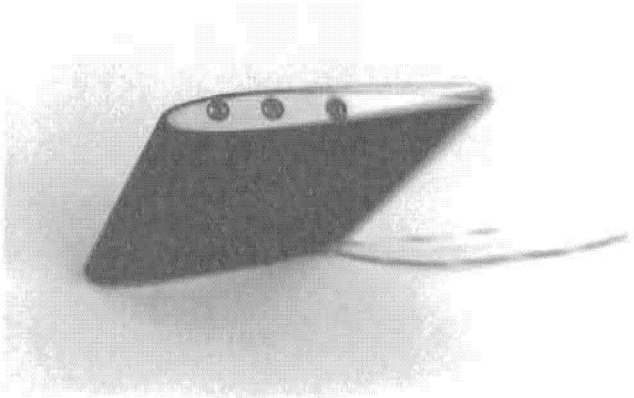

Figure 12. DAP torque fin mounted in wing tunnel undergoing ±2.2° Pitch deflections at 40 m s^{-1} airspeed.

±45°. This applies both to DAP actuator plies and the composite substrate.

It is possible to integrate an active torque plate into a missile fin such that significant twist deflections are obtained. A fin measuring 66 mm by 93 mm generates static pitch deflections in excess of ±3°. Because the fin has its elastic axis 5%c behind the quarter-chord, these deflections are shown to grow with increasing airspeed. These active deflections can be predicted within 6% once the stiffness of the torque plate and the lift-curve slope of the wing are known.

Acknowledgments

The author wishes to express his sincere appreciation to the University of Kansas Aerospace Engineering Department for providing laboratory space and to Dr David Downing and the Kansas Space Grant Consortium, funded by NASA Headquarters, for providing him with support. The guidance of Dr Nesbitt Hagood of MIT on modeling principles and properties of piezoelectric fiber composites is also appreciated. The author also wishes to acknowledge the support of his wife, Karin, for tolerating the endless hours spent in the laboratory.

Appendix. Nomenclature

A	= extensional stiffness matrix
B	= coupling stiffness matrix
c	= wing chord
D	= bending stiffness matrix
d_{31}	= piezoelectric extension-charge coupling coefficient
d_{36}	= piezoelectric in-plane shear-charge coefficient
E	= modulus of elasticity
E_3	= actuation potential
G	= shear modulus
L	= length of DAP element
N	= applied force per unit length
M	= applied moment per unit length
OR	= orthotropy ratio = $E_{\text{Leff}}/E_{\text{Teff}}$
t	= thickness
V	= volume fraction
u, v, w	= element deflections in the x, y, z directions
W	= width of DAP element
α	= angle of attack
δ	= control surface deflection
ϵ	= in-plane strain
ϵ^0	= mid-plane strain
κ	= plate curvature
Λ	= free piezoelectric element active strain
ν	= Poisson's ratio
Θ	= ply orientation angle
σ	= ply stress

Subscripts

11, 22...	= tensor notation subscripts
a	= actuator
b	= bond layer
eff	= effective (due to combined attachment methods)
effo	= original effective (due to attachment geometry)

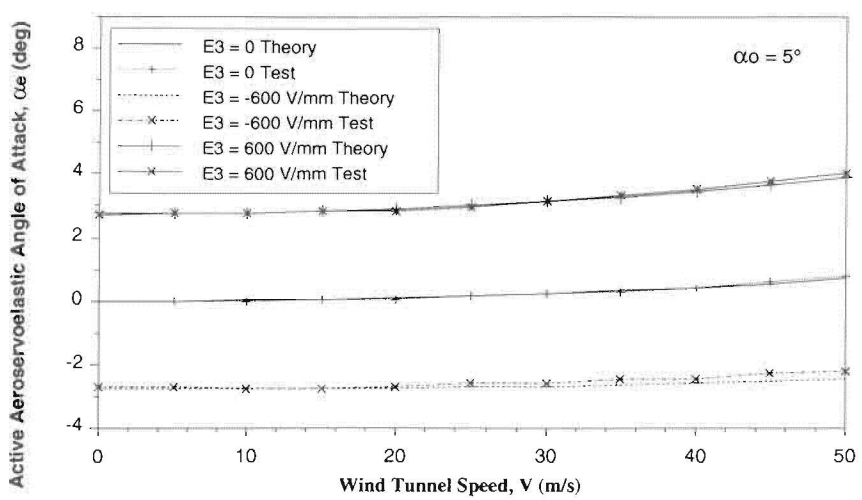

Figure 13. Wind tunnel test data of aeroservoelastic DAP fin.

f = fiber
l = laminate
m = matrix
o = original (without any attachment effects)
s = substrate.

References

[1] Lacau R G 1988 A survey of missile aerodynamics *Proc. NEAR Conf. on Missile Aerodynamics (Monterey, California, 1988)* ed M R Mendenhall *et al* (Mountain View, CA: Nielsen Engineering and Research) pp 1.1–1.54

[2] 1991 *Improved Sidewinder Extended Combat Effectiveness, Performance and Reliability* (Missile Systems Division, Raytheon Corporation, Bedford, MA)

[3] Wood M E 1988 Application of experimental techniques to store release problems, *Proc. NEAR Conf. on Missile Aerodynamics (Monterey, California, 1988)* ed M R Mendenhall *et al* (Mountain View, CA: Nielsen Engineering and Research) pp 5.1–5.44

[4] Crawley E F, Lazarus K B and Warkentin D J 1989 Embedded actuation and processing in intelligent materials *2nd Int. Workshop on Composite Materials and Structures for Rotorcraft (Troy, New York, September, 1989)*

[5] Ehlers S M and Weisshaar T A 1990 Static aeroelastic behavior of an adaptive laminated piezoelectric composite wing *Proc. 31st AIAA/ASME/ASCE/AHS/ASC Structures, Structural Dynamics and Materials Conf. (Long Beach, CA, April 2–4 1990) Paper no AAIAA-90-1078-CP* (Washington, DC: AIAA)

[6] Song O Lobrescu L and Rogers C A 1991 Static aeroelasticity behaviour of adaptive aircraft wing structures modeled as composite thin-walled beams *Forum Aeroelasticity and Structural Dynamics (Aachen, Germany, 1991)*

[7] Spangler R L and Hall S R 1990 Piezoelectric actuators for helicopter rotor control *Proc. 31st AIAA/ASME/ASCE/AHS/ASC Structures, Structural Dynamics and Materials Conf. (Long Beach, CA, April 2–4 1990) Paper no* (Washington, DC: AIAA)

[8] Lazarus K B Crawley E F and Bohlmann J D 1990 Static aeroelastic control using strain actuated adaptive structures *Proc. 1st Joint US/Japan Conf. on Adaptive Structures (Maui, Hawaii, October 1990)*

[9] Ehlers S M and Weisshaar T A 1992 Effect of material properties on static aeroelastic control *33rd Structures, Structural Dynamics and Materials conf. (Dallas, Texas, 15 April 1992)*

[10] Barrett R M 1990 Intelligent rotor blade and structural development using directionally attached piezoelectric crystals *MS Thesis* University of Maryland

[11] Barrett R M 1990 Intelligent rotor blade actuation through directionally attached piezoelectric crystals *Paper presented at 46th AHS Forum for the Lichten Competition (Washington, DC, 1990)*

[12] Barrett R M 1990 Method and apparatus for structural actuation and sensing in a desired direction *US Patent Application* 485 599/07

[13] Chopra I 1991 Development of and intelligent rotor *Conf. on Active Materials and Adaptive Structures (Alexandria, Virginia, November 1991)* ed G J Knowles (Bristol: Institute of Physics) p 271

[14] Barrett R M 1992 Actuation strain decoupling through enhanced directional attachment in plates and aerodynamic surfaces *Proc. 1st European Conf. on Smart Structures and Materials (Glasgow, May 1992)* ed B Culshaw *et al* (Bristol: Institute of Physics) pp 383–6

[15] Barrett R M 1992 Active plate and wing research using EDAP elements *Smart Mater. Struct.* 1 214–26

[16] Barrett R M 199X Active plate and missile wing development using DAP elements *AIAA J.* at press

[17] Jones R M 1975 Micromechanical behavior of a lamina *Mechanics of Composite Materials* (New York: Hemisphere)

[18] Ekvall J C 1965 Structural behavior monofilament composites *Proc. 6th AIAA Structures and Materials Conf. (New York, April 1965)*

[19] KYNAR® 1987 *Piezo Film Product Summary and Price List* (Pennwalt Corporation)

[20] Kinsley R S *et al* 1990 Piezoceramic application data *Piezo Systems Product Catalog* (Cambridge, MA: Piezo Systems Inc.)